PAPER

Optimising composite viscosity leads to high sensitivity electromechancial sensors

To cite this article: Daniel P O'Driscoll *et al* 2018 *2D Mater.* **5** 035042

2D Materials

PAPER

RECEIVED
12 April 2018

REVISED
26 May 2018

ACCEPTED FOR PUBLICATION
11 June 2018

PUBLISHED
27 June 2018

Optimising composite viscosity leads to high sensitivity electromechancial sensors

Daniel P O'Driscoll, Victor Vega-Mayoral, Ian Harley, Conor S Boland and Jonathan N Coleman

School of Physics and CRANN & AMBER Research Centers, Trinity College Dublin, Dublin 2, Ireland

E-mail: bolandc1@tcd.ie and colemaj@tcd.ie

Keywords: graphene, nanocomposites, electromechanics, viscosity

Abstract

To realise real-time, wearable personal health monitors, sensitive, low stiffness, inexpensive smart materials must be identified. Previously, room-temperature, low-viscosity nanocomposites based on graphene-doped Silly Putty (*G*-putty) were demonstrated. Displaying unprecedented electromechanical sensitivity and physical properties, *G*-putty is an ideal material to fill this niche. However, the relationship between processing conditions or indeed material properties and sensitivity is not known. Herein, we study the relationship between a number of processing parameters and the electromechanical properties of *G*-putty. We identify the processing conditions required to produce *G*-putty with gauge factors >100. In addition, we found a well-defined relationship between composite viscosity and sensitivity which shows maximised gauge factors for viscosities ~4×10^5 Pa · s.

Introduction

The addition of nanomaterials to polymers to form composite materials with enhanced mechanical, barrier and electrical properties has been extensively investigated over the last two decades [1–4]. Recently, attention has turned to the electromechanical properties of nanocomposites. For conductive nanocomposites, the electrical properties can change on application of an applied strain, ε, such that (at low strain) the fractional resistance change is given by [5]:

$$\frac{\Delta R}{R_0} = \left[\frac{1}{\rho_0}\frac{\mathrm{d}\rho(\varepsilon)}{\mathrm{d}\varepsilon} + 2\right]\varepsilon = G\varepsilon \qquad (1)$$

where $\rho(\varepsilon)$ is the resistivity under strain and ρ_0 is the zero-strain resistivity. In nanocomposites, the resistivity can change significantly under strain due to tunnelling or connectivity effects leading to potentially very large values of $\mathrm{d}\rho/d\varepsilon$ [5]. This makes such materials very useful as strain sensors. The sensing response is usually described by the sensitivity metric known as the gauge factor (G). In recent times, a wide range of organic [6–11] and inorganic [12–14] nanomaterials have been used as strain sensing materials, with graphene-filled composites [11, 15–19] being of particular interest. Although such materials have shown great promise as real-time kinaesthetic [6] and vital signs [7] monitors, mostly their performances have been limited to values of $G < 100$ [6, 20]. To realise more sensitive materials, some aspect of the nanocomposites must be improved.

Recently, our work on graphene-loaded viscoelastic nanocomposites using a low viscosity polymer matrix, polysiloxane crosslinked by boric acid (commonly known as Silly Putty), was shown as a possible way forward [5]. The resultant composite material, *G*-putty, displayed values of G as high as 1000. However, the method for *G*-putty production reported was un-optimised and inefficient, resulting in low *G*-putty yields. In addition, when using such an unrefined method, it is unclear what material properties or synthesis factors are important for maximising G and thus realising *G*-putty's full potential. Here, we show a systematic, optimised and scalable method for producing the highly electromechanically sensitive nanocomposite material, *G*-putty. Composite properties were characterised as a function of cross-linker concentration, curing time, and molecular weight of starting material. Varying these input parameters led to significant changes in the electrical and mechanical properties of the composites and allowed us to identify the conditions required to maximise G. In addition, we found a clear link between G and composite viscosity.

Results and discussion

Graphene was prepared by liquid phase exfoliation [21–23] through the sonication of graphite at high concentration in the solvent N-methyl-pyrrolidone [24–26]. The subsequent graphene slurry formed was then centrifuged to remove all large unexfoliated aggregates, after which, the supernatant was decanted. The resultant dispersion was then filtered onto a filter membrane to form a thick film of graphene. This film was then redispersed by tip sonication in chloroform to form a stock graphene dispersion [24, 25]. In figure 1(A), a TEM image of the flakes redispersed in chloroform can be seen. All flakes are noted to have relatively large lateral sizes, between 50 and 1000 nm (figure 1(B)), and are expected to be 1–6 monolayers thick [25].

Previously, home-made silly putty was made by mixing silicone oil and boric acid (B.A), a mild cross-linker, on a hotplate to form a polysiloxane [5]. As the reaction was heated only from the bottom of the vessel, and the heat only distributed by a magnetic stirrer bar, this led to significant temperature variations in the reaction vessel. As a result of this inefficient heating, the curing of the oil was difficult to control with this method. Compounded by the fact that only one sample could be made at a time, the hot plate method is less than ideal for optimisation tests and thus must be improved. This motivated the development of a more refined setup, in which up to six reaction vessels can be placed in a custom made aluminium holder which sits in a temperature controlled oil bath. The resultant putty (without graphene) formed using this new method was indistinguishable in colour and consistency from putty previously reported using the hotplate method [5]. Using the process described here, a maximum yield of ~10 g of pristine putty can be produced at one time; compared to ~1.5 g for the hot plate method.

As per our previous work, the home-made putty was transferred to a vessel containing a graphene:chloroform dispersion and mixed (see Methods) to form *G*-putty. The resultant composite was black in colour and mechanically more robust than pristine putty. However, it still remained relatively soft and malleable [5] and can be shown to easily hold formed shapes (figure 1(C)). To confirm the composition of the *G*-putty, we performed Raman spectroscopy on both pristine putty and *G*-putty (figure 1(E)). While the putty spectrum displayed the expected PDMS modes below 1000 cm^{-1} (not shown) and between 2800 and 3000 cm^{-1}, the *G*-putty spectrum contained identical bands but also showed the characteristic D, *G* and 2D bands associated with graphene. Subtracting the putty spectrum from the *G*-putty spectrum (after normalising to the main PDMS peak) yielded a spectrum (blue line) which is exactly as expected for liquid phase exfoliated graphene [23]. This indicates that the graphene nanosheets are intact after composite formation and interact relatively weakly with the polymer matrix.

Using the new processing method for *G*-putty, we explored varying a number of processing parameters with the aim of developing control over the electromechanical sensitivity via the intrinsic material properties. We identified the B.A concentration, curing time and molecular weight of the constituent PDMS Oil as the most promising parameters to vary. In all cases of the study, the graphene content of our samples was kept constant at 15 wt%.

For all samples of *G*-putty made, we measured the zero-strain conductivity, σ, before performing tensile tests where we strained the sample (10 mm min^{-1} to 20% strain) while measuring stress and resistance simultaneously (N.B. trying to remain close to the standard notation, we refer to conductivity as σ. However, this symbol is also commonly used for stress. To minimise confusion, we will refer to stress below as σ_m). Using $R-\varepsilon$ data, the gauge factor can be obtained from the slope of the $\Delta R/R_0$ versus ε graph (at low strain). In addition, we fitted the stress–strain curves using the Standard linear solid model (SLS) which described the mechanical properties of a combination of springs and a dashpot (figure 2(A) inset) [5, 27]. The SLS predicts that for a viscoelastic material, the stress, σ_m, is related to strain by:

$$\sigma_m = E_2\varepsilon + \eta\dot{\varepsilon}\left(1 - e^{-\varepsilon/\dot{\varepsilon}\tau}\right) \quad (2)$$

where $\dot{\varepsilon}$ is the strain rate, η is the viscosity, $\tau = \eta/E_1$ is the relaxation time and E_1 and E_2 are the elastic moduli associated with the pair of springs used in this model [5]. Previously, we demonstrated that, for *G*-putty, the parameters extracted from fitting stress–strain curves using this model match those found with other methods, e.g. rheology or stress-relaxation measurements [5].

Our first set of experiments, described in figure 2, show the properties of *G*-putty produced using different concentrations of B.A (with curing time and oil M_n (number average molecular weight) kept constant at 150 min and 26 000 g mol^{-1}). Shown in figure 2(A) are stress strain curves for putty produced with two B.A concentrations and the associated SLS fits. In all cases, good fits were found and η, E_1 and E_2 extracted.

We can see the effect of varying B.A concentration on the three parameters of the SLS model in figures 2(B)–(D). A plot of composite viscosity as a function of B. A concentration in figure B shows a 100-fold increase in composite viscosity from ~10^5 to ~10^7 Pa · s when increasing cross-linker concentration from 0.2 g ml^{-1} to 0.6 g ml^{-1}. This is to be expected, as by increasing the amount of B. A present in the material we increase the number of sites available for the formation of temporal crosslinks. In this case the crosslinks come from two separate interactions: (i) Si–O–B–O–Si linkages which form via a condensation reaction between the −OH group terminals of the PDMS

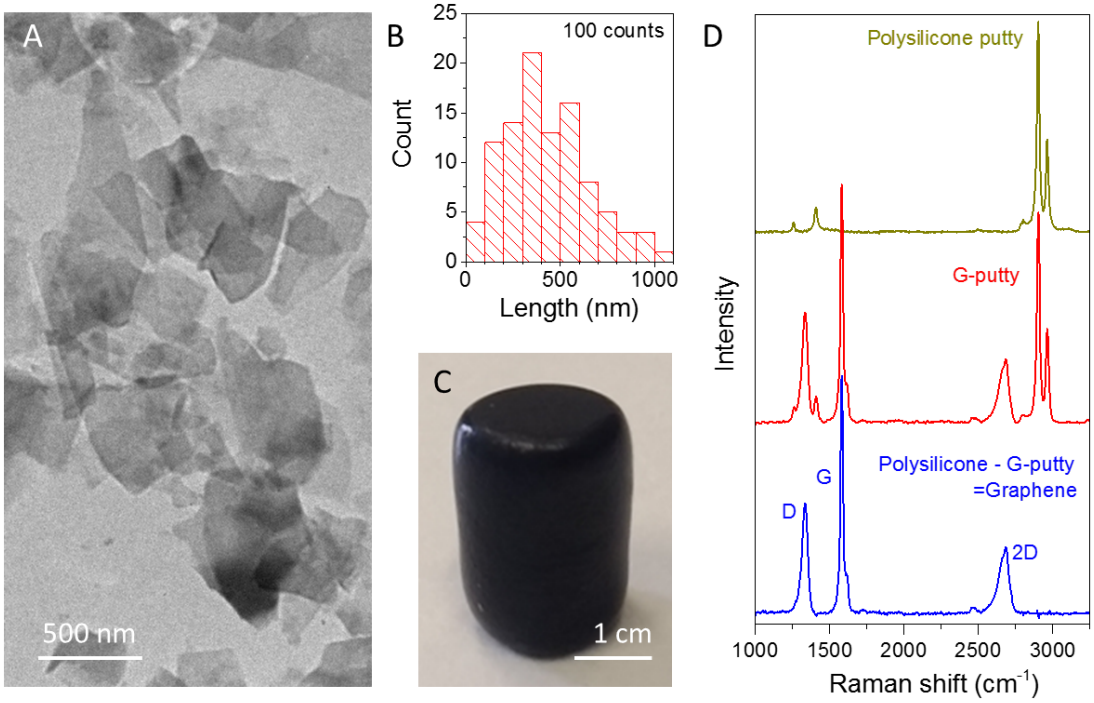

Figure 1. (A) TEM image of liquid exfoliated graphene nanosheets. (B) Histogram showing distribution of nanosheet lengths. (C) Photograph of *G*-putty (15 wt% graphene) hand moulded into a cylinder. (E) Raman spectra measured on polysilicone putty (green) and *G*-putty (red). These spectra have been normalised to the polysilicone mode at 2900 cm^{-1}. The blue spectrum represents the difference between these spectra and is consistent with the spectrum of liquid exfoliated graphene nanosheets.

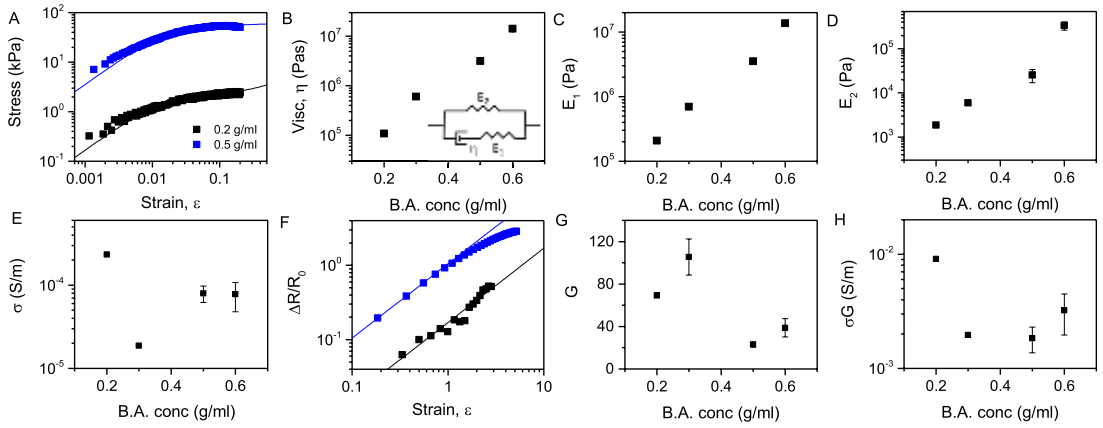

Figure 2. Properties of *G*-putty produced using a range of B.A concentrations (curing time and oil M_n kept constant at 150 min and 26 000 g mol^{-1}). (A) Representative stress strain curves for *G*-putty with two different B.A concentrations. Solid lines represent fits to the standard SLS which represents the combination of springs and dashpot shown in (B) expressed mathematically via equation (2). The parameters, η, E_1 and E_2, associated with these fits are plotted versus the (B). concentration in (B)–(D) (data points averaged over fits to curves measured for 3–5 samples). (E) Zero-strain conductivity of *G*-putty plotted versus B.A concentration. (F) Fractional resistance increase plotted as a function of strain for *G*-puttys fabricated with two different B.A concentrations. The solid lines represent linearity. (G) *G*-putty strain-sensing sensitivity factor, *G*, plotted, versus B.A concentrations. (H) Product of σG plotted versus B.A concentrations.

chains and the B.A. (ii) The B.A in these linkages also have −OH groups attached to a central boron atom. The OH groups can weakly interact with each other via hydrogen bonding leading to the formation of temporary bonds which break and reform on the timescales of ~1 s [27].

By increasing the degree of crosslinking, we limit the mobility of the polymer chains. This would be expected to lead to an increase in composite viscosity. Indeed, as the B.A. content is increased from 0.2 to 0.6 g l^{-1}, the viscosity is seen to increase from ~10^5 to ~10^7 Pa (figure 2(B)). This is accompanied by large increases (roughly 100-fold) in the elastic parameters E_1 and E_2 (figures 2(C) and (D)). Increases in stiffness with B.A. concentration are to be expected by analogy with cross-linked elastomers. For example, the affine network model predicts the stiffness of a cross-linked polymer to scale with the cross link density [28]. It is clear that the B.A content has a significant effect on the composite mechanical properties.

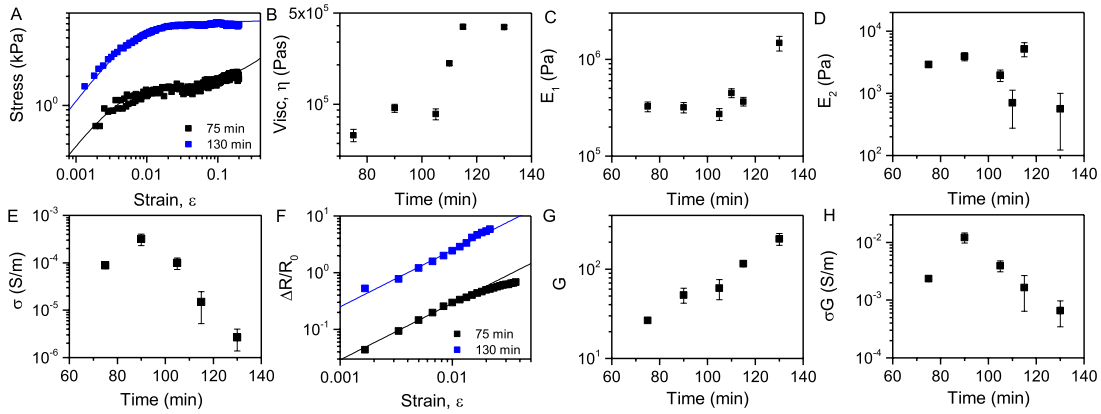

Figure 3. Properties of *G*-putty produced with a range of curing times (B.A concentrations and oil M_n kept constant at 0.4 g ml^{-1} and 13 700 g mol^{-1}). (A) Representative stress strain curves for *G*-putty with two different curing times. Solid lines represent fits to the standard SLS expressed mathematically via equation (2). The parameters, η, E_1 and E_2, associated with these fits are plotted versus the curing time in (B)–(D) (data points averaged over fits to curves measured for 3–5 samples). (E) Zero-strain conductivity of *G*-putty plotted versus curing time. (F) Fractional resistance increase plotted as a function of strain for *G*-puttys fabricated with two different curing times. The solid lines represent linearity. (G) *G*-putty strain-sensing sensitivity factor, *G*, plotted, versus curing time. (H) Product of σG plotted versus curing time.

As previously shown, the addition of graphene to home-made silly putty yields a composite that is electrically conductive [5]. However, it is not clear how the B.A. content would impact the conductivity. To test this, electrical characterisation was carried out for the same range of B.A concentrations as was described above. As shown in figure 2(E), conductivity was found to decrease slightly from 10^{-3} S m^{-1} to 10^{-4} S m^{-1} with increasing B.A concentration. We hypothesise that this decrease in conductivity is linked to the reduction in nanosheet mobility with increasing cross-link density. Previously, we observed a non-trivial mobility of graphene nanosheets in polysilicone matrices, leading to spontaneous reorganisation of deformed nanosheet networks into more isotropic arrangements with higher conductivity [5]. It is likely that the increased composite viscosity at higher B.A contents leads to reduced nanosheet mobility, which restricts the development of networks which are optimised for electrical conductivity. By increasing the amount of cross-linking, we limit the movement of the sheets and their ability to form contact junctions, thereby keeping the resistance at a higher level resulting in a lower conductivity [5].

We also performed electromechanical tests for *G*-putty with different B.A. contents by measuring the resistance as a function of tensile strain. Typical plots are presented in figure 2(F) as the fractional resistance as a function of strain. In all cases we focused on the low-strain region in order to measure the gauge factor, *G*. We note that at higher strains we would expect to observe a reduction in resistance due to network relaxation (nanosheet mobility) effects [5]. For all electromechanical tests, the composite, resistance was observed to increase with applied strain in line with equation(1). In each case the gauge factor was extracted with the obtained values plotted versus B.A content in figure 2(G). Although the data was scattered, we found the gauge factor to fall with increasing B.A. content from ~100 to ~30 over the experimental range.

We note that, in addition to high *G*, electromechanical sensors must have conductivity which is high enough to facilitate conductivity measurement. As a result, in addition to *G*, it is important to consider the product of *G* and the composite conductivity, σ, as a parameter which carries information about both sensitivity and current carrying capability. Plotting the product of *G* and σ as a function of B.A concentration, values are seen to drop from ~10^{-2} S m^{-1} to ~ 10^{-3} S m^{-1} at ~0.3 g ml^{-1}; remaining at a constant value after this point. This however, is merely a reflection of the fall in conductivity with B.A concentration previously noted.

Similar tests were carried out on samples where the properties of the *G*-Putty were recorded as a function of the curing time (figure 3). In these experiments, the B.A concentration was kept constant at 0.4 g ml^{-1} and the molecular weight of the oil at 13 700 g mol^{-1}. The stress strain curves were again fitted with the SLS model (equation(2)) in figure 3(A). The parameters derived from the fit are shown in figures 3(B)–(D) as a function of the curing time. Similar to the effects of increasing the B.A concentration in the composite, the viscosity of the composite showed a steady increase from 5×10^4 to 5×10^5 Pa · s as the curing time is increased from 70 to 130 min. This may be linked to the decreased chain mobility associated with an increase in cross-link density with curing time. In figure 3(C), E_1 remains relatively invariant for the majority of the cure times at 3×10^5 Pa before increasing suddenly at ~110 min by almost an order of magnitude to 2×10^6 Pa. Conversely, as shown in figure 3(D), we see an overall decrease in E_2 at long curing times.

The conductivity of the *G*-putty for different cure times is plotted in figure 3(E) and shows an increase

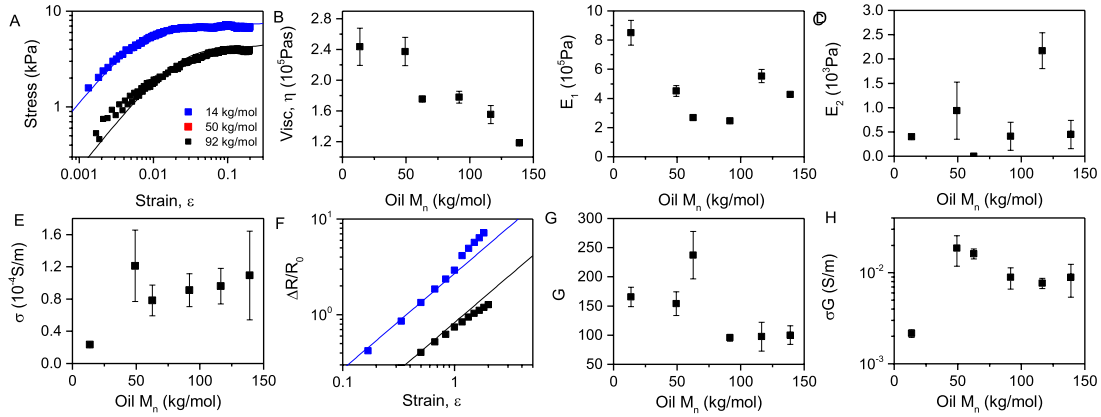

Figure 4. Properties of *G*-putty produced with a range of silicone oil molecular weights (B.A concentrations and curing time kept constant at 0.4 g ml^{-1} and 130 min). (A) Representative stress strain curves for *G*-putty with two different oil M_n. Solid lines represent fits to the standard SLS expressed mathematically via equation(2). The parameters, η, E_1 and E_2, associated with these fits are plotted versus the oil M_n in (B)–(D) (data points averaged over fits to curves measured for 3–5 samples). (E) Zero-strain conductivity of *G*-putty plotted versus oil M_n. (F) Fractional resistance increase plotted as a function of strain for *G*-puttys fabricated with two different oil M_n. The solid lines represent linearity. (G) *G*-putty strain-sensing sensitivity factor, *G*, plotted, versus oil M_n. (H) Product of σG plotted versus oil M_n.

from 10^{-4} S m^{-1} for a cure time of 70 min to a distinct peak of 4×10^{-4} S m^{-1} at ~90 min. With further curing, σ is found to drop to ~10^{-6} S m^{-1} at 130 min. From figure 3(E), it is evident that there is an optimum curing time for *G*-putty at which conductivity can be maximised. Looking at the electromechanical response of the composites in figure 3(F), gauge factor can again be extracted for samples with different curing time. Plotting *G* as a function of curing time in figure 3(G), a continuous increase from *G* ~25 to ~120 is observed, implying that, in this range at least, the increase in cross-link density achieved with increasing curing time results in increased sensing sensitivity. However, by plotting $G \cdot \sigma$ against cure time in figure 3(H), we see a similar trend in the data as to that of the conductivity plot in figure 3(G). Values increase from 10^{-3} S m^{-1} at 70 min to a peak value of 10^{-2} S m^{-1} at ~90 min, after which values decrease to 10^{-4} S m^{-1} at 130 min. This shows that when considering both the requirements of high sensitivity and conductivity, there may be an optimum curing time.

Finally, the molecular weight of the constituent PDMS oil was varied. The B.A concentration was kept constant at 0.4 g ml^{-1} and the curing time was kept constant at 130 min while the oil M_n (number average molecular weight) was varied from 13.7 to 139 kg mol^{-1}. In figure 4(A), stress strain curves obtained from tensile tests of the *G*-Putty made from a range of different molecular weight oils are shown. This was again fitted using equation (2), with the SLS parameters plotted as a function of the molecular weight of the oil in figures 4(B)–(D). Figure 4(B) shows that the viscosity of the composites as a function of the constituent oil molecular weight decreased from 4×10^5 Pa · s at ~10^4 g mol^{-1} to ~10^5 Pa · s at ~10^5 g mol^{-1}. This apparently counter-intuitive result is due to the reduction in the number of chain ends with increasing M_n, resulting in a reduction of scope for cross-linking (which is dominated by reactions at chain ends) [29]. This is also reflected in figure 4(C), as we see a significant decrease in E_1 from 2×10^5 Pa to 2×10^4 Pa with increasing M_n. However, in figure 4(D), E_2 remains relatively invariant with M_n at ~10^3 Pa.

In figure 4(E), a significant increase in conductivity is seen when increasing M_n from ~10^4 to 5×10^4 Pa. Values for σ are found to jump from ~10^{-6} to 10^{-4} S m^{-1}, remaining unchanged for all M_n past this point. Resistance-strain curves for selected values of oil M_n are shown in figure 4(F). The extracted gauge factor was found to decrease from *G* ~180 to ~100 (figure 4(G)) over the same M_n range. Plotting the product of $G \cdot \sigma$ in figure 4(H), the conductivity trend again dominates the shape of the plot. Values increase dramatically from 10^{-3} S m^{-1} for a 10^4 g mol^{-1} base oil to 10^{-2} S m^{-1} for a 5×10^4 g mol^{-1} oil, with values for $G \cdot \sigma$ remaining unchanged for higher M_n oils.

While the data above gives indications of the local dependence of output parameters (conductivity; η; E_1; E_2; and *G*) on input parameters (t, B.A conc and M_n), it cannot show the overall behaviour in a multiparameter system such as this. In order to attempt to identify more global trends, we prepared a large number of additional *G*-putty samples with various combinations of input parameters. We then plotted each of the output parameters versus each of the input parameters as shown in figure 5. We note that in all panels, each data point is described by a combination of input parameters rather than having two input parameters fixed and varying the other. Although, this approach is somewhat limiting, it has the advantage that it can make clear global trends or lack thereof. For example, the lack of clear trends shows that none of the output parameters (i.e. *G*-putty properties such as η or *G*) show a well-defined dependence on either B.A conc or M_n. However, the situation is slightly different for the curing time, t. Although no very well defined trend

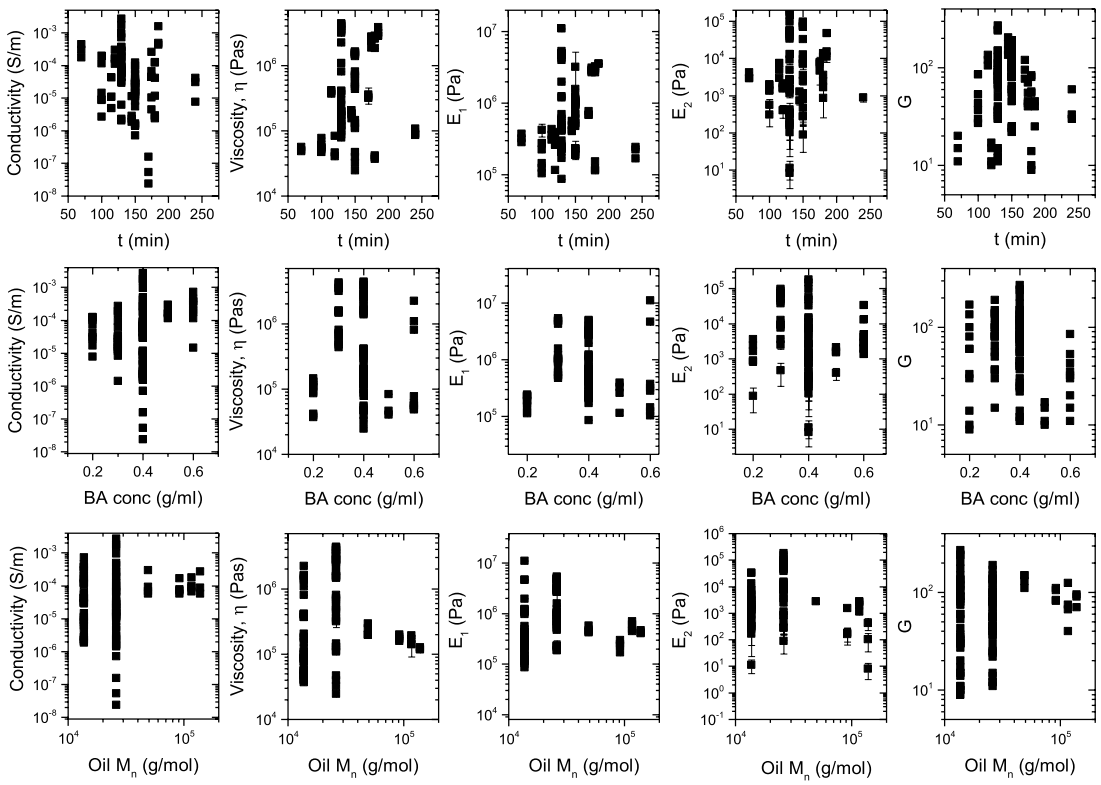

Figure 5. Plots of output parameters; conductivity; viscosity, η; E_1; E_2; and gauge factor, G; versus input parameters; curing time, t; B.A concentration, B.A conc; and silicone oil molecular weight, M_n. In all cases, the data points represent various combinations of t, B.A conc and M_n.

is observed, the composite conductivity appears to be minimised for values of t ~ 150–175 min while the other four output parameters appear to be maximised at the same curing time. While the nature of this effect is not clear, it does show the absolute importance in optimising curing time in these systems.

Another important point is that all five output parameters vary very widely over the range of input parameters with maximum variation ranging from $\times 30$ for G to $\times 10^5$ for conductivity. This is of great interest as, for composites, each of these properties would generally be expected to be fixed by the graphene content. Here, the graphene content is fixed (15 wt% in each case) showing that local variation is polymer morphology or network structure can play a very significant role in composite performance. This is most clear for conductivity which is extremely sensitive to connectivity of the nanosheet network, both on large scales, where the network must efficiently span the sample, but also on smaller scales where the charge must be able to easily pass from sheet to sheet. This data makes clear that the details of the composite processing have a great impact on network connectivity.

The G putty with the highest observed G-value ($G = 270$) was prepared using a curing time of 130 min, a B.A concentration of 0.4 g ml^{-1} and an oil molecular weight of 13 700 g mol^{-1}. However, it is likely that similar combinations of input parameters would yield similar properties. In order to identify the best combinations of input parameters, we plotted histrograms showing the values of input parameters which led to G-putties with $G > 100$ (figure 6). This graph clearly shows that low oil molecular weight (~10^4 g mol^{-1}) combined with B.A. concentrations close to 0.4 g mol^{-1} and curing times in the region of 150 min gave the best results. This data should make it possible to achieve further optimisation of G-putties.

The fact that both gauge factor and viscosity follow similar trends with curing time (figure 5) is interesting because of our previous observation that these parameters might be linked [5]. To test this, we plot gauge factor versus G-putty viscosity for the entire sample set in figure 7(A). We find a very well defined relationship, characterised by a peak in G for composite viscosities close to 4×10^5 Pa · s with a maximum observed G-value of ~300, in line with our similar report of $G = 500$ in optimised systems [5]. We note that we would expect to achieve lower values of G here as the graphene loading level used here was quite far from the percolation threshold. This highlights the importance of optimising the global composite properties if G is to be maximised. This is underlined by the fact that G-values as low as 10 were observed for both high- and low-viscosity composites.

Previously, viscosity was solely controlled by varying the content of graphene contained in an individual composite sample. It was shown that at a particular critical loading level of graphene, G-putty would undergo gelation [5]. This liquid-solid transition was described by a percolation-like behaviour in electrical

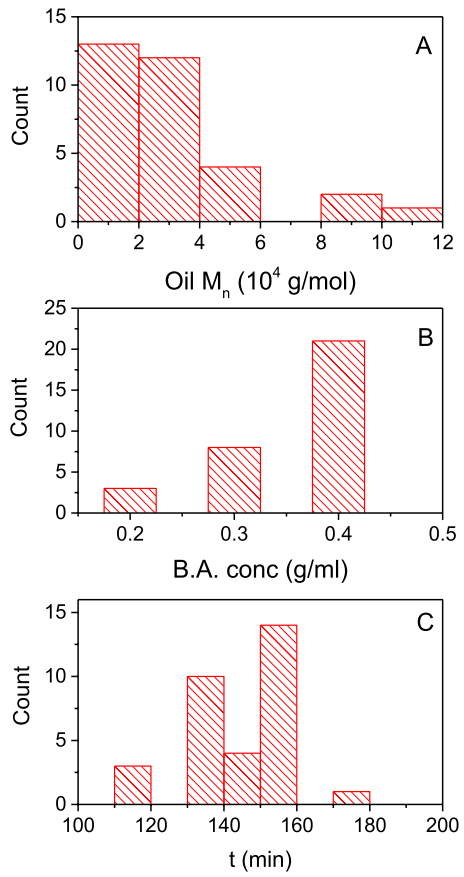

Figure 6. Histograms showing input parameters ((A), oil molecular weight; (B) B.A concentration; (C) curing time) for the 32 batches of *G*-putty which displayed $G \geqslant 100$.

relaxation times which diverged either side of this critical loading level, known as the gelation point [30]. Around this point, the corresponding values for *G* were at their largest and subsequently fell according to a power law with decreasing relaxation times, i.e. increasing composite viscosities [5]. Similarly, looking at figure 7(A), though viscosity was varied using production method variations the same divergent like behaviour can be seen around $\sim 10^5$ Pa · s, the previously reported viscosity at which gelation occurred for *G*-putty [5].

In addition, the data in figure 5 suggests a negative correlation between *G* and conductivity. This is illustrated in figure 7(B) where we plot *G* versus conductivity over the entire data set, finding a clear fall-off in *G* with increasing conductivity. The negative correlation between gauge factor and composite conductivity is well known in strain sensors. This global behaviour is consistent with a scaling of the form $G \propto \sigma^{-1/3}$ (dashed line). Interestingly, this scaling is identical to the $G \propto R^{1/3}$ (where *R* is resistance) scaling reported by Hempel *et al* for spray coated graphene-only networks [31]. The falloff in *G* with conductivity is usually discussed in terms of filler content, where the gauge factor is usually reported as increasing as the percolation threshold is approached. However, in this work, all samples have the same graphene content. This means that our observation of *G* decreasing with increasing conductivity cannot be explained by both properties scaling with filler loading level. Combined with Hempel's data, this implies a direct relationship between *G* and conductivity. In addition, in these composites, this behaviour illustrates the significant variation of network connectivity in these samples which lead to variations in both *G* and conductivity even while the graphene content is fixed.

Conclusions

In this work we have both systematically and randomly varied the processing (input) parameters associated with the fabrication of graphene-polysilicone composites (*G*-putty). For each combination of input parameters we have measured a number of output parameters, the conductivity and electromechanical gauge factor as well as mechanical parameters. We find that even though the graphene content is kept constant in these composites, the composite properties (output parameters) vary very strongly as the input parameters are varied. The data suggests that the processing parameters have a significant effect on the connectivity of the nanosheet network. In addition, we observe well defined relationships between gauge factor and both viscosity and conductivity.

Methods

The production of *G*-putty consists of two steps: (i) Making pristine home-made putty (ii) Infusion of grapheme. In step one, B.A and silicone oil are reacted to form the viscoelastic material known commercially as 'Silly Putty'. The B.A used was supplied by Sigma Aldrich (99.999% trace metal basis CAS# 10043-35-3). This was done for a range of B.A concentrations ranging from 0.3 to 0.7 g ml^{-1}. A range of different molecular weight silicone oils were used and were specified by their manufacturer in the terms of their kinematic viscosity (mm^2 s^{-1}). This was converted into number average molecular weight (g mol^{-1}) using the AJ Barry formula which is appropriate for linear polysiloxanes [32]. The range of silicone oils were as follows: 350 mm^2 s^{-1}—VWR CAS #63148-62-9, 1000 mm^2 s^{-1}—Clearco CAS#63148-62-9, 5000 mm^2 s^{-1}—Clearco CAS#63148-62-9, 10 000 mm^2 s^{-1}—Clearco CAS#63148-62-9, 30 000 mm^2 s^{-1}—Sigma Aldrich CAS#63148-62-9, 60 000 mm^2 s^{-1}—Sigma Aldrich CAS#63148-62-9, 100 000 mm^2 s^{-1}—Sigma Aldrich CAS#63148-62-9.

2 mls of silicone oil of a particular molecular weight was added to a 28 ml vial. The B.A was first milled using a mortar and pestle to break up any large crystals and facilitate reactivity. Once a fine powder was formed it was added to the silicone oil. This was done for a variety of concentrations ranging from 300 to 700 mg ml^{-1}. The mixture was then stirred at room temperature until homogenous and an opaque, milky

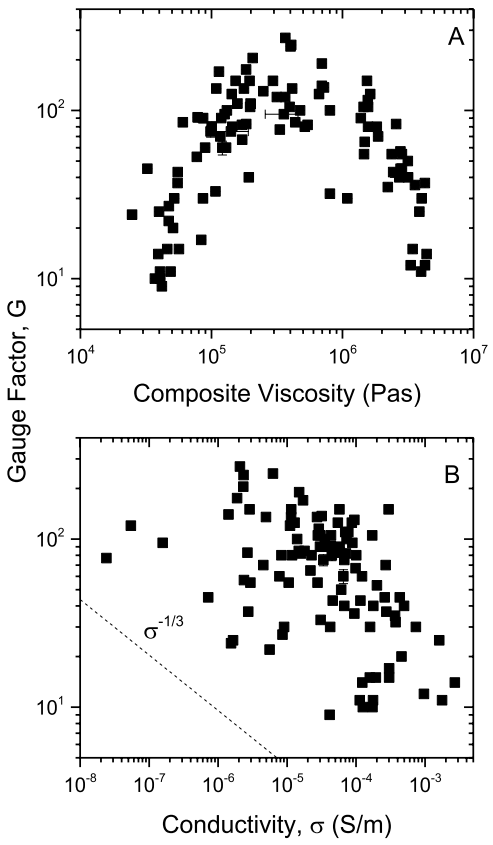

Figure 7. Composite gauge factor, *G*, plotted versus (A) composite viscosity, η, and (B) composite conductivity. In (B), the dashed line represents $\sigma^{-1/3}$ behaviour.

substance was formed. The vials were added six at a time to a specially designed aluminium holder.

An oil bath was preheated to 160 °C using an IKA C-MAG HS 7 hotplate. The temperature was controlled and monitored using a ETS—D5 thermometer. The holder was then partially submerged in the oil bath and the temperature increased to 225 °C over a period of ~15 min. This warm up period is included in the curing times discussed in the 'Results and Discussion'. The mixture was stirred continuously via a magnetic stirrer bar placed in each of the vials. The vials were then allowed to heat for a designated curing time. Once the mixture was finished heating, the holder was removed from the oil bath and allowed to cool. The resultant material is a gum-like substance which turns into the viscoelastic putty after cooling.

Graphene was prepared by liquid phase exfoliation. Graphite was added to the solvent N-methylpyrrolidone (NMP) at a concentration of 100 mg ml^{-1} and sonicated for 72 h at 50% amplitude. The mixture was then centrifuged at 1500 rpm for 90 min in order to remove any large unexfoliated graphite particulates and large flakes. This produced a dispersion with a mean flake size of 430 ± 20 nm. The dispersion was then vacuum filtered onto a 0.4 μm pore size nylon membrane to form a thick graphene film. This film was then broken apart and added to chloroform at a concentration of 10 mg ml^{-1} then redispersed using tip sonicated for ~2 h at 40% amplitude.

800 mgs of the pristine putty was placed in a beaker with 14.5 mls of graphene/chloroform dispersion. The mixture was heated (~50 °C) and stirred gradually on a hotplate making sure that the putty had dispersed completely forming a homogenous mixture. The solvent was evaporated off until a thick, viscous liquid is formed in the beaker. The beaker was then left to air dry ~12 h in a fume hood to remove the remaining solvent. Once the solvent had fully evaporated a thick black/grey film was left on the bottom of the vessel, *G*-putty. The putty was then removed with a spatula.

Raman spectroscopy was performed with a Horiba Jobin Yvon LabRAM HR800 with 633 nm excitation laser in air under ambient conditions. The Raman emission was collected by 100× objective lens (N.A. = 0.8) and dispersed by a 600 line mm^{-1} grating using 10% of the laser power (~2 mW). A total of 3–5 spectra, collected at different positions on both the pristine putty and *G*-putty, were baseline-corrected and averaged.

Electro-mechanical measurements were performed on putty samples using a Keithley KE2601 source meter in a 2-probe mode, controlled by LabView software, in conjunction with a Zwick Z0.5 ProLine Tensile Tester (100 N Load Cell). Test samples were hand-rolled into the desired shape with dimensions measured using an electronic Vernier callipers. For electro-mechanical tensile tests, specimens with a gauge length of L0 = 9 mm and a diameter of D0 = 2.2 mm were strained at a rate of typically 10 mm min^{-1} up to 20% strain. The clamps of the tensile tester were used as electrical contacts and were attached to the source meter via wire leads.

Acknowledgments

This work was primarily funded by the European Union Seventh Framework Program under grant agreement n°604391 Graphene Flagship but was also supported via the Science Foundation Ireland (SFI) funded centre AMBER (SFI/12/RC/2278).

ORCID iDs

Daniel P O'Driscoll https://orcid.org/0000-0001-8306-0700
Victor Vega-Mayoral https://orcid.org/0000-0001-8626-0775
Ian Harley https://orcid.org/0000-0002-6668-3794
Conor S Boland https://orcid.org/0000-0003-4376-6770
Jonathan N Coleman https://orcid.org/0000-0001-9659-9721

References

[1] Zhu Y *et al* 2010 Graphene and graphene oxide: synthesis, properties, and applications *Adv. Mater.* **22** 3906–24
[2] Young R J *et al* 2012 The mechanics of graphene nanocomposites: a review *Compos. Sci. Technol.* **72** 1459–76

[3] Gong S and Cheng W 2017 One-dimensional nanomaterials for soft electronics *Adv. Electron. Mater.* **3** 1600314
[4] Luo Q *et al* 2018 All-carbon-electrode-based endurable flexible perovskite solar cells *Adv. Funct. Mater.* **28** 1706777
[5] Boland C S *et al* 2016 Sensitive electromechanical sensors using viscoelastic graphene-polymer nanocomposites *Science* **354** 1257
[6] Boland C S *et al* 2014 Sensitive, high-strain, high-rate bodily motion sensors based on graphene-rubber composites *ACS Nano* **8** 8819–30
[7] Samad Y A *et al* 2015 Novel graphene foam composite with adjustable sensitivity for sensor applications *ACS Appl. Mater. Interfaces* **7** 9195–202
[8] Liu H *et al* 2016 Electrically conductive thermoplastic elastomer nanocomposites at ultralow graphene loading levels for strain sensor applications *J. Mater. Chem.* C **4** 157–66
[9] Yamada T *et al* 2011 A stretchable carbon nanotube strain sensor for human-motion detection *Nat. Nanotechnol.* **6** 296–301
[10] Yin G *et al* 2011 A carbon nanotube/polymer strain sensor with linear and anti-symmetric piezoresistivity *J. Compos. Mater.* **45** 1315–23
[11] Qin Y *et al* 2015 Lightweight, superelastic, and mechanically flexible graphene/polyimide nanocomposite foam for strain sensor application *ACS Nano* **9** 8933–41
[12] Boland C S *et al* 2017 Surface coatings of silver nanowires lead to effective, high conductivity, high-strain, ultrathin sensors *Nanoscale* **9** 18507–15
[13] Cheng Y *et al* 2017 Stretchable electronic skin based on silver nanowire composite fiber electrodes for sensing pressure, proximity, and multidirectional strain *Nanoscale* **9** 3834–42
[14] Ho M D *et al* 2017 Percolating network of ultrathin gold nanowires and silver nanowires toward 'invisible' wearable sensors for detecting emotional expression and apexcardiogram *Adv. Funct. Mater.* **27** 1700845
[15] Chun S, Choi Y and Park W 2017 All-graphene strain sensor on soft substrate *Carbon* **116** 753–9
[16] Li X, Hua T and Xu B 2017 Electromechanical properties of a yarn strain sensor with graphene-sheath/polyurethane-core *Carbon* **118** 686–98
[17] Nakamura A *et al* 2017 A piezo-resistive graphene strain sensor with a hollow cylindrical geometry *Mater. Sci. Eng.* B **219** 20–7
[18] Ren J *et al* 2017 Environmentally-friendly conductive cotton fabric as flexible strain sensor based on hot press reduced graphene oxide *Carbon* **111** 622–30
[19] Yao H B *et al* 2013 A flexible and highly pressure-sensitive graphene-polyurethane sponge based on fractured microstructure design *Adv. Mater.* **25** 6692–8
[20] Amjadi M *et al* 2016 Stretchable, skin-mountable, and wearable strain sensors and their potential applications: a review *Adv. Funct. Mater.* **26** 1678–98
[21] Hernandez Y *et al* 2009 High-yield production of graphene by liquid-phase exfoliation of graphite *Nat. Nanotechnol.* **3** 563–8
[22] Coleman J N 2009 Liquid-phase exfoliation of nanotubes and graphene *Adv. Funct. Mater.* **19** 3680–95
[23] Paton K R *et al* 2014 Scalable production of large quantities of defect-free few-layer graphene by shear exfoliation in liquids *Nat. Mater.* **13** 624–30
[24] Khan U *et al* 2010 High-concentration solvent exfoliation of graphene *Small* **6** 864–71
[25] Khan U *et al* 2011 Solvent-exfoliated graphene at extremely high concentration *Langmuir* **27** 9077–82
[26] Coleman J N 2013 Liquid exfoliation of defect-free graphene *Acc. Chem. Res.* **46** 14–22
[27] Cross R 2012 Elastic and viscous properties of Silly Putty *Am. J. Phys.* **80** 870–5
[28] Rubenstein M and Colby R H 2003 *Polymer Physics* (Oxford: Oxford University Press)
[29] Lobkov V D, Klebanskii A L and Kogan E V 1965 Boric acid-induced reactions of polydimethylsiloxanes *Polym. Sci. USSR* **7** 1699–703
[30] Winter H H and Mours M 1997 Rheology of polymers near liquid–solid transitions *Neutron Spin Echo Spectroscopy Viscoelasticity Rheology* (Berlin: Springer) pp 165–234
[31] Hempel M *et al* 2012 A novel class of strain gauges based on layered percolative films of 2D materials *Nano Lett.* **12** 5714–8
[32] Barry A J 1946 Viscometric investigation of dimethylsiloxane polymers *J. Appl. Phys.* **17** 1020–4